

Review

# Enhancement of Surface Properties Using Ultrashort-Pulsed-Laser Texturing: A Review

Reem A. Alsaigh

Department of Physics and Astronomy, College of Science, King Saud University, Riyadh 11451, Saudi Arabia; rsaigh@ksu.edu.sa

**Abstract:** Surface texturing, which has recently garnered increased attention, involves modifying the surface texture of materials to enhance their tribology. Various methods have been developed for surface texturing. Laser surface texturing (LST) has attracted considerable interest because of its excellent texturing accuracy, controllability, and flexibility. It improves surface wettability properties and increases the wear resistance of materials while reducing the coefficient of friction. Herein, we present an overview of the underlying mechanisms of interactions between short-pulsed lasers and materials. In addition, we review published studies on the effects of LST on surface properties, including surface roughness, wettability, friction, and wear resistance. We believe that this review will provide valuable insights into the recent advances in surface property enhancement through LST, which exhibits potential for various applications.

**Keywords:** laser surface texturing; wettability; surface roughness; coefficient of friction; wear resistance

## 1. Introduction

Ultrashort-pulsed lasers have provided new options for enhancing the surface properties of materials because they can be employed to manipulate the processing of materials from the microscale to the nanoscale or across scales [1]. Lasers exhibiting various energy intensities and pulse durations are used to change processes and cause phenomena [2]. However, the application of long and nanosecond pulses in the traditional pulsed-laser processing of materials results in expansive heat-affected zones (HAZs), thermal-shock cracks, recast layers, and dross accumulation at the entrances and exits of drilled microholes, holes with high aspect ratios (width/depth ratios), morphology changes, and related damage. In recent years, researchers have started favoring ultrashort-pulsed lasers that operate in the picosecond and femtosecond (fs) regimes to address the abovementioned constraints. The advantages of these lasers include considerable repeatability, fine geometrical-feature control, and minimal HAZs. Further, pulsed fs lasers are primarily used in fields such as the automotive, medical, and aerospace fields as well as microelectronics and photonics for surface modification, drilling, and cutting various materials. As a unique laser machining technique, fs-laser surface texturing (fs-LST) is used for enhancing the tribological, biological, optical, and wetting performances of surfaces. Customized surfaces can be created with excellent accuracy using this method [3].

Laser-material interactions primarily involve three components: early ultrafast events that occur in response to the laser-induced excitation of optically active electronic states in the involved exposed material; rapid nonequilibrium phase changes induced through energy transmission from energized electrons to atomic vibrations; and cooling and solidification of the target surface area after radiation exposure [4].

This article provides a short overview of laser-induced excitation and nonthermal processes that occur within electronically excited materials. We then discuss laser ablation and summarize surface property enhancement through surface texturing.



**Citation:** Alsaigh, R.A. Enhancement of Surface Properties Using Ultrashort-Pulsed-Laser Texturing: A Review. *Crystals* **2024**, *14*, 353. <https://doi.org/10.3390/cryst14040353>

Academic Editors: Qinghua Wang and Chunfang Guo

Received: 6 March 2024

Revised: 5 April 2024

Accepted: 6 April 2024

Published: 9 April 2024



**Copyright:** © 2024 by the author. Licensee MDPI, Basel, Switzerland. This article is an open access article distributed under the terms and conditions of the Creative Commons Attribution (CC BY) license (<https://creativecommons.org/licenses/by/4.0/>).

## 2. Laser–Solid Interactions

### 2.1. Metals

Metallic materials have abundant free electrons. With regard to metallic materials, absorption primarily occurs through free–free transitions. When the interaction of an fs laser with a metallic material starts, free electrons absorb photon energy, increasing their kinetic energy, thereby increasing their temperature [5]. With an increasing number of heated electrons, their interactions with the involved lattice enhance, eventually heating the lattice. Subsequently, a transition phase occurs over a time range of picoseconds to tens of nanoseconds, producing plasma for microseconds to milliseconds [1].

### 2.2. Semiconductors

Unlike metallic materials, semiconductor materials lack sufficient free electrons; most electrons are in bound states in the valence band. With regard to semiconductor materials, valence electrons are primarily energized to the conduction band through the absorption of individual photons when the photon energy exceeds the bandgap. Multiphoton absorption becomes substantial when the direct-bandgap energy exceeds the involved photon energy [6]. Given the probability that multiphoton absorption has a power law relation with laser intensity, absorption is predictable and sensitive to laser intensity; it corresponds to considerably short laser pulses, which have substantially high intensities because of low pulse durations [4]. In this case, valence band electrons absorb multiple photons and move to the conduction band, where they become free electrons. Consequently, electron–hole pairs can be generated [1]. Laser-induced electron–hole pairs have considerable kinetic energy ( $E_g = h\nu$ ), which is immediately transferred to lattice vibrations, heating the involved semiconductor [5]. This process is called multiphoton ionization [1]. A schematic of the multiphoton ionization process is shown in Figure 1a. When the electric field generated by a femtosecond laser reaches a certain strength, it significantly weakens the Coulomb field that holds a valence electron to its nucleus. As a result, the electron becomes effectively liberated and can tunnel through the potential barrier, as shown in Figure 1b, in a phenomenon known as tunneling ionization. This process is a prominent feature of femtosecond laser interaction with matter under conditions of strong laser fields and low laser frequencies.

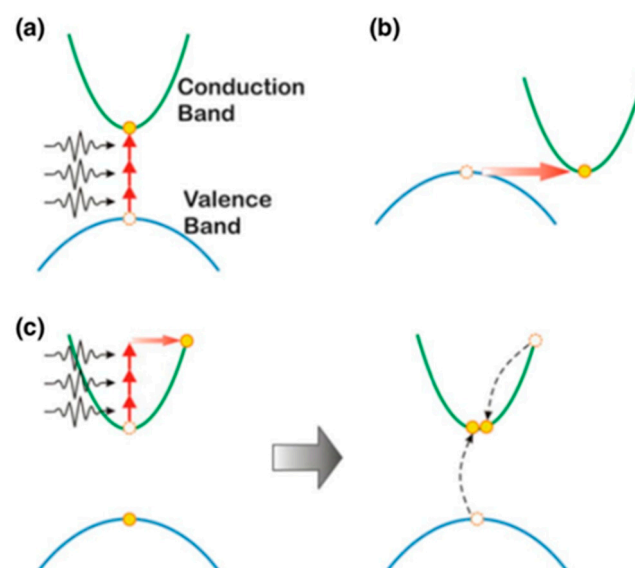


**Figure 1.** A schematic representation of multiphoton ionization (a), tunnel ionization (b), and avalanche ionization (c) [1].

When several photons are absorbed by free electrons, multiphoton ionization results in low–high energy transitions in the conduction band; thus, a free electron gains additional kinetic energy and collides with a valence electron. In this case, energy transfer occurs to

produce two free electrons with low energy levels, as shown in Figure 1c. These free electrons absorb photons and collide with valence electrons, initiating an avalanche-like chain reaction; this process is called impact ionization or avalanche ionization [1,7]. Multiphoton ionization and avalanche ionization are highly nonlinear processes [8].

Lattice-free electron interactions may considerably modify interatomic bonding and lead to a phase change [4,9,10]. When the temperature of the involved material reaches the melting or vaporization point after laser-material interactions, the material changes its state from solid to liquid, gas, or plasma [5]. These phase transitions are nonthermal because, upon direct laser-induced excitation, they occur in electronically excited states in a few picoseconds and do not require electron-phonon equilibration or lattice heating [4].

### 2.3. Insulators

Insulating materials have a large energy bandgap, requiring sufficiently high laser intensity for multiphoton absorption. Therefore, the production of a large concentration of free electrons in the conduction band, which causes the interactions of insulating materials with photons to resemble those of metals and semiconductors, is possible [5].

## 3. Ultrashort-Pulsed-Laser Ablation

As an important physical effect of fs lasers, ablation involves direct material removal from an object of interest through laser light absorption. During laser machining, the target material absorbs the involved laser beam and melts or evaporates, causing morphological changes in and around the absorption zone [3]. After laser energy absorption, the heating, melting, and vaporization of the material cause phase transitions.

As a primary factor in the assessment of laser precision engineering, the HAZs are influenced by laser settings, such as fluence, pulse duration, absorption coefficient, and target materials. They are large during laser irradiation with pulse durations longer than a few picoseconds because electrons require nanoseconds to transfer energy to the lattice, resulting in high material temperatures. Additionally, heat action causes material expulsion from the surface [5], leaving the contact area for expansion through collateral effects such as formations of microcracks, burrs, and recast layers, which reduce machining precision. In this case, ablation is the transition from solid to liquid and then to gas [3]. For fs pulses lasting  $<10^{-13}$  s, the transfer of the absorbed energy from electrons to the lattice within such a brief relaxation time is prevented. Therefore, the local electron temperature can only increase because of electron-electron interactions, and the HAZs are small. Given the extremely short processing time, fs laser ablation can be considered a direct solid-vapor or solid-plasma transition. Here, the lattice is heated in picoseconds, causing the involved vapor and plasma to quickly expand. Consequently, surface ablation caused by an fs laser leads to a small HAZ [5]. Figure 2a shows the notable molten layer present when steel is exposed to (a) nanosecond radiation. In contrast, the exact ablation caused by fs radiation leaves no traces of the involved molten material (Figure 2b). The fluence of the ablation threshold for a given material decreases and becomes increasingly distinct with decreasing pulse durations [11].

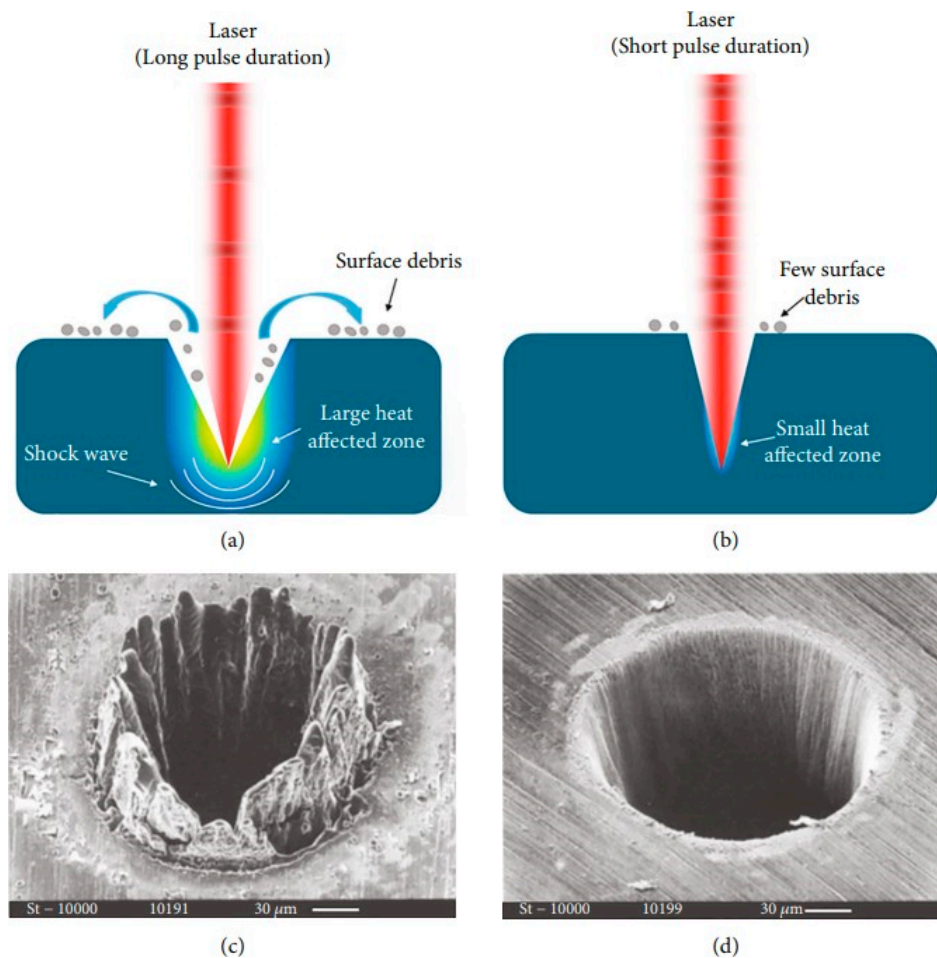


**Figure 2.** Interaction of a laser with a material for various pulse durations: (a) long and (b) short pulse durations. SEM images of laser-ablated holes fabricated on a 100- $\mu\text{m}$  steel foil using a (c) 780 nm laser (pulse duration: 3.3 ns and energy density:  $0.5 \text{ J}/\text{cm}^2$ ) and (d) 780 nm laser (pulse duration: 200 fs and energy density:  $0.5 \text{ J}/\text{cm}^2$ ) [5].

#### 4. Ultrashort-Pulsed-LST

Surface ablation through laser pulses creates holes with depths of several nanometers to micrometers. Regular laser-formed surface structures, ranging from simple periodic segments to dimples in polygonal or hierarchical patterns, can be created using ultrashort laser pulses with repetitive laser-beam movements. This approach of laser-based periodic-object production is called LST. Given its use of a coherent beam, LST offers inherent benefits such as high accuracy, simple operation, cleanliness, and rapid processing. It has applications in various domains, including tribology, material engineering, wettability improvement, brazing, medicine, and optics [12–16]. LST is used to create precise microconvex arrays, microdimples, and microgrooves on the surfaces of materials (Figure 3). It is an efficient and popular technique that can be employed to alter interactions between surfaces to improve surface roughness and lubrication, reducing friction, and increasing material wear resistance. Laser surface processing has garnered considerable interest owing to its distinct advantages, such as speed, effectiveness, controllability, and the capacity to create extremely complex surface textures [17].

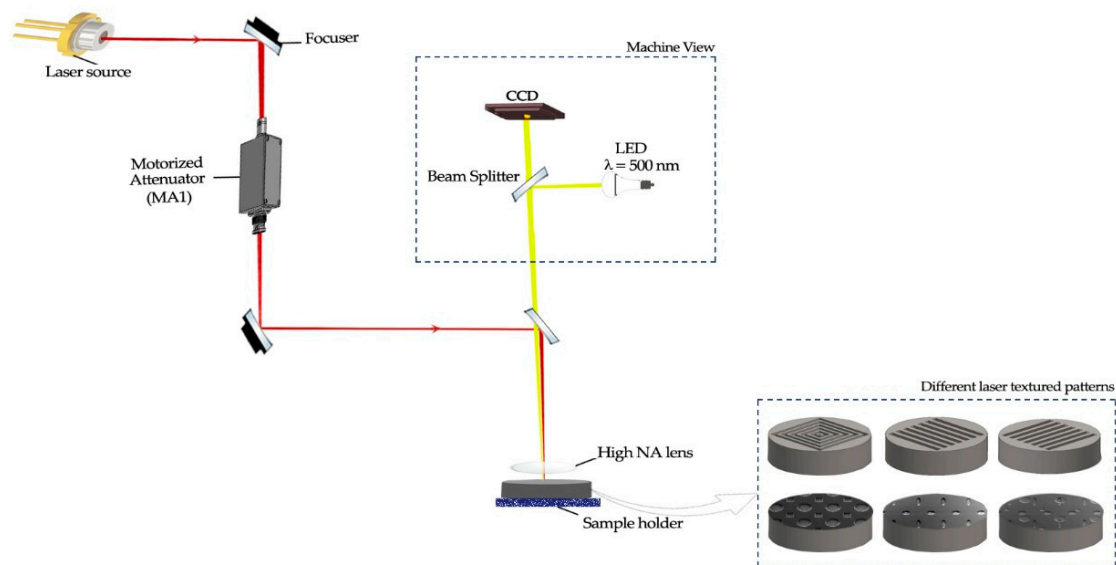


Figure 3. Laser surface texturing.

## 5. Wettability and Surface Roughness

Moldovan et al. [18] used LST to modify the wettability and surface roughness of ferritic stainless steel (AISI 430). The involved laser had an Nd: fiber active medium with an average power of 20 W, a wavelength of 1064 nm, and a pulse frequency of 5–1000 kHz. Three designs of AISI 430 ferritic stainless steel were considered: type A, which was donut-shaped with three concentric octagonal designs; type B, which had a 90° angle between two ellipses; and type C, which comprised a collection of craters, holes, and dimples. LST was accomplished by adding portions that resembled grooves and varied in depth. Contrary to the involved processing speed, the spot density (number of repetitions) was directly associated with the surface roughness. Substantial data indicated that the type-A design demonstrated hydrophobicity, with the average contact angle (CA) being constant during processing. For the type-B design,  $\geq 20$  repetitions were required to achieve optimal hydrophobicity. Meanwhile, hydrophilicity was attained by the type-B design through  $< 20$  repetitions. The rule associated with the number of repetitions required to achieve specific properties was different for the type-C design than for the other designs. Notably, the average static CAs of the designs appeared to slightly decrease with an increasing number of repetitions. Further, the frequency had a remarkable effect on the average static CAs. The average static CAs for the type-B and -C designs were  $\leq 90^\circ$  when operated at frequencies of  $< 40$  kHz. The results of the wettability analysis of LST areas enabled the elucidation of the wettability effects of frequency and number of repetitions. With an increasing number of repetitions for a constant frequency, the observed static CA increased, providing hydrophobicity to the microstructural surface (Surfaces with CAs of  $< 90^\circ$  are hydrophilic,  $> 90^\circ$  are hydrophobic and  $> 150^\circ$  are superhydrophobic, as explained in Figure 4). Conversely, with increasing frequency for a constant number of repetitions, the static CA decreased. Ahmed et al. [19] investigated LST for austenitic stainless steel (AISI 304). They used a Ti-sapphire laser with a maximum energy of 200  $\mu\text{J}$ , pulse duration of 30 fs, and frequency of 10 kHz to create three textures: square, parallel, and perpendicular textures. The treated surfaces were distinguished based on their wettability, microhardness, surface roughness, and phase structure. Further, the tribological performances of the textured and untextured samples were examined using a ball-on-disk tribometer. Results revealed the formation of a highly hydrophilic surface for all textures. The square, parallel, and perpendicular textures provided CAs of approximately 22.2°, 22.8°, and 23.2°, respectively. Changes in the chemical compositions of AISI 304 austenitic stainless steel, with the number of repetitions kept fixed to a value obtained from the study by Moldovan et al. [18], changed

the surface wettability. In addition, fs-LST demonstrated the ability to reduce the rate of wear and the coefficient of friction (COF). In particular, when slipping in a dry environment, the smooth texture exhibited a COF of 0.22; meanwhile, the parallel and perpendicular textures exhibited COFs of 0.13 and 0.14, respectively. Therefore, the COFs of the samples with the perpendicular, parallel, and square textures were overall 36%, 40%, and 68% lesser, respectively, than that of the untextured sample. The wear rates of the samples with the square, parallel, and perpendicular textures were approximately 22%, 37%, and 50%, respectively, lower than that of the untextured sample. Wang et al. [20] employed a simple laser-based surface texturing technique to exert switchable wettability control on a titanium surface. The wettability of the treated surface could be efficiently changed multiple times between superhydrophilicity and superhydrophobicity by alternating between 355 nm UV-based LST and low-temperature heat treatment, respectively. The used laser had a 20 ns pulse width, 30 kHz repetition rate, 14.7 W average power, and 0.5 mJ pulse energy. A crosshatch design was used because of its simplicity and excellent manufacturing efficiency. The untreated Ti surface exhibited a CA of 75.3°. After texturing, the CA of the laser-textured Ti surface reduced to 0°, resulting in superhydrophilicity. The CA of the heat-treated laser-textured surface increased to 153.2° after 2 h of heat treatment, resulting in a superhydrophobic surface. Subsequently, exposing the laser-textured Ti surface to UV light for 4 h reversed its CA to 0 °C. This effect caused all the textured surfaces to again become superhydrophilic. Ten superhydrophobicity–superhydrophilicity cycles improved the stability and repeatability of the wettability control of the laser-textured Ti surface. The experimental findings showed that laser texturing quickly caused the surfaces to become superhydrophilic. Prakash et al. [21] used an Nd:YAG picosecond laser operating at 3 W, 532 nm, and 45 kHz to produce texture on a Ni-based superalloy (C-263) to investigate surface roughness and wetting behavior. Four wave-pattern combinations were applied to the sample surface using the Nd:YAG laser. Different power values, scanning speeds, and pass numbers were used to obtain the required geometric pattern. Comparing the textured and untextured surfaces revealed that the surface roughness of the textured surface increased by 92%. A high overlapping ratio, minimum width, and maximum pitch were combined to improve the surface roughness ratio. Elemental analysis revealed that over 21 d, the overlap of pulses, power, frequency, and scanning speed had a remarkable effect on the formation of oxygen and carbon molecules. The wetting characteristic of the textured surface changed from hydrophilic to hydrophobic because of the presence of carbon and oxygen molecules. Sierra et al. [22] studied the change in the wettability properties of Ti–6Al–4V using a fiber-based nanosecond pulsed laser to generate micropillars on the sample surface. The material was irradiated by a laser with a pulse width of 65 ns, a repetition rate of 65 kHz, a scanning speed of 260 mm/s, and six fluences (4.07, 5.09, 6.11, 7.13, 8.14, and 9.17 J/cm<sup>2</sup>) with four lines (50, 100, 150, and 200 μm). The results demonstrated that using fluences of 5.09 and 6.11 J/cm<sup>2</sup> was the most effective way to establish a superhydrophobic system. Bizi-Bandoki et al. [23] exposed AISI 316L stainless steel and Ti–6Al–V alloys to fs laser pulses with varying pulse numbers to improve the involved surface topography and wettability. A total of 150 fs pulses with a 5 kHz repetition rate, constant frequency, 0.2 W average power, and 2.04 J/cm<sup>2</sup> fluence were delivered by a Ti–sapphire laser system. The wettability and surface topography of four samples for each alloy gradually altered through exposure to different numbers of pulses (13, 32, 84, and 128). A multiscale morphology comprising nanoperiodic and microperiodic ripples was created and modified by varying the pulse number, resulting in modifications of the wetting properties. Before laser irradiation, the surfaces of 316L steel and TA6 V were hydrophilic with average CAs of 79.5° and 75°, respectively. The CA presented a global increase because of the increase in pulses. The CA of the TA6V sample increased from 98° to 124.6° at N = 128 pulses. AISI 316L samples exhibited the same progression of CA, i.e., their CA increased from 92.4° to 116.5° under 13 and 84 pulse treatments. However, an atypical hydrophilic behavior, instead of an increase in the CA, reappeared because of the roughness scale when a pulse number of 128 was selected. Therefore, the number of pulses increased

the perceived CAs; hydrophilic materials became hydrophobic. Chen et al. [16] examined how texturing the Ti alloy surface with an fs laser could improve wetting behavior during the laser welding–brazing of a Ti/Al butt joint. The morphology and wetting behavior of the Ti surface and structural patterns created by fs-LST were examined for different laser powers. After fs laser processing, a 6061 Al alloy was used to solder Ti–6Al–4V alloys with treated and untreated surfaces through laser welding–brazing. The following optimal focused laser parameters were used: an offset of 1 mm on the Al side, a laser power of 3 kW, and a welding speed of 1.2 m/min. The surface morphology of the Ti–6Al–4V alloy was considerably affected by the process parameters of the fs laser. Among the surfaces, the surface with a stripe pattern textured with a 1.5 W laser revealed the lowest roughness of 1.0145  $\mu\text{m}$ . The surface morphology of Ti surfaces textured using an fs laser was associated with wetting and spreading behaviors. With increasing laser power to texture the surface of Ti–6Al–4V with a stripe pattern, the CA first increased and subsequently decreased. The lowest CA value of 4.6° was obtained at a 1.5 W laser power. The textured surfaces with circular (27.8°) and grid (29.9°) shapes showed comparable CAs when exposed to water. A CA of 25.7° was obtained when TiZrNiCu (brazing filler metals) contacted the unpatterned surface of Ti–6Al–4V. The CA of TiZrNiCu decreased to 10.1° when a striped pattern and 1.5 W laser power were used to texture the Ti–6Al–4V surface. AgCu and Al foil are brazing filler metals with CAs of 10.4° and 9.7°, respectively. The surface microstructure of Ti–6Al–4V exhibited increased hydrophilic capabilities after fs-LST and diverse behavior with different microstructures. This result differs from the findings of two previous studies on the same material. These studies indicated that changing the laser fluence and pulse number changed the surface from hydrophilic to hydrophobic. Gemini et al. [24] employed fs-LST to produce superhydrophobic surfaces on mirror-polished 316L steel. They applied fs-infrared-LST with fluences per pulse of 0.36, 1.14, and 2.33 J/cm<sup>2</sup> and repetition rates from 100 to 1000 kHz and created numerous morphologies using various process settings. Low fluence per pulse reduced the spatial periodicity of laser-induced periodic surface structures (LIPSSs) to less than the laser wavelength. LIPSSs are based on the direct self-organization of materials and enable the creation of certain microstructures and nanostructures on large surfaces. As the repetition rate increased at the same fluence, the induction of thermal effects on the creation of the microstructure resulted in the formation of microgrooves with high spatial periodicity. With additional increases in fluence per pulse and repetition rate, the morphology changed from a homogenous net of circular holes with an average diameter of <5  $\mu\text{m}$  to defined columnar structures with an average size of tens of  $\mu\text{m}$ . After a few days, the texture of the surface changed from hydrophilic to hydrophobic, and in the event of laser processing at the greatest repetition rate, it became superhydrophobic. CA values of >120° were obtained in the low-fluence regime within a few days after laser processing, whereas surfaces exhibited hydrophilic behavior in the low-repetition-rate regime. Yusuf et al. [25] studied the effect of using LST on a TiO<sub>2</sub>-coated surface for generating a self-cleaning surface. Before laser texturing, a TiO<sub>2</sub> coating was applied on a carbon steel API substrate using a plasma spray. The TiO<sub>2</sub> surface was textured with microdimples using a Q-switched Nd:YAG picosecond laser. The area density, dimple depth, and dimple diameter were 20 m, 7 m, and 0.2%, respectively. The findings indicated that the nontextured TiO<sub>2</sub> coating exhibited a CA of 58.5° and was hydrophilic. Following laser texturing, all samples exhibited superhydrophilic behavior. The author attributed this result to the modification of the chemical composition and morphology of the sample surfaces by laser texturing. Baron et al. [26] employed LIPSSs to create intricate biomimetic patterns on the surface of steel 1.7131. Patterns were created after exposure to fast-repeating fs laser pulses. An fs Yb-doped fiber with a maximum output power of 40 W, laser wavelength of 1030 nm, and pulse duration of 340 fs was used. Several irradiation factors, including laser fluence and repetition rate, were examined to generate the necessary structural data with an emphasis on the effects of the laser scanning frequency on the same area. In this investigation, more than half of the produced surfaces exhibited wetting behavior with CAs of 92° ± 2°–136° ± 6°. Surfaces with CAs of >150°

are superhydrophobic. Chen et al. [27] examined the effects of CVD diamond material on its surface roughness (arithmetic-mean height of a line, or Sa, and maximum height, or Sz) and ablation depth to enhance the overall quality of machined surfaces. They developed an energy density distribution (EDD) model to describe the microstructural alterations in CVD diamond material following laser machining. They used a pulsed Yt-doped fiber nanosecond laser with the following specifications: fixed laser duration of 100 ns, maximum average power of 20 W, wavelength of 1064 nm, and maximum repetition rate of 200 kHz. The variance in surface roughness and ablation depth at various laser parametric settings was assessed by employing the EDD model. In this research, the primary goal of laser machining of a specific material, CVD diamond, is to cause graphitization before material removal. The exploratory experiment indicated that CVD diamond could be graphitized when the average laser power exceeded 3 W and could be efficiently graphitized at 7 W. Graphitization was guaranteed by employing low levels of laser filling pitch and scanning speed. The findings revealed that the surface roughness values Sa and Sz increased with increasing average laser power and decreased with increasing laser scanning speed and filling pitch; however, abnormalities occurred at a scanning speed of 30 mm/s and a filling pitch of 3 m. Kumar and Soni [28] exposed a single crystalline InP to a nanosecond pulsed Nd–YAG laser beam at the fourth harmonic wavelength (266 nm) in an HF electrolyte to create a submicrometer-sized laser-induced periodic surface structure (ripples). The ripples were oriented in line with the laser polarization direction. The surface was modified using a Q-switched Nd:YAG laser operating at 266 nm (fourth-harmonic wavelength) with a 10 Hz pulse repetition rate (PRR), 125 mJ/cm<sup>2</sup> energy density, and a pulse width of 5 ns. The InP surface ripple structure developed as the number of laser shots increased from 200 to 600 in aqueous HF. Power spectral density (PSD) and cross-sectional analyses were performed to understand the effect of changing the number of laser shots on the surface morphology of the ripples. PSD analysis revealed that with an increasing number of laser shots, the roughness increased and the ripple structure periodicity decreased. Jalil et al. [29] investigated the effect of fs-LST on the hydrophobicity and bacterial adhesion properties of Au surfaces. With the aid of the raster scanning of the laser beam at different laser fluences, they produced various structures, including conic and 1D rod-like structures, spherical nanostructures, and subwavelength fs-LIPSSs that covered nanostructures and microstructures. A Ti:sapphire amplifier fs laser with a 1 kHz repetition rate, an 800 nm central wavelength, and a 30 fs pulse duration was used as the irradiation source to create microstructures/nanostructures on the surface of Au. The laser fluence varied from 0.08 to 3 J/cm<sup>2</sup>, whereas the laser processing parameters, such as scanning speed, focal spot distance, and interspacing between two scanned lines, were fixed at optimal values. Results showed that treating Au with fs-LIPSSs caused its initially hydrophilic unpatterned surface with a CA of 74° to change to a hydrophobic surface, i.e., fs-LIPSSs 108°. The hydrophobicity of the fs-LIPSSs covered with nanostructures increased to 122°. With nanorods/microrods, cones, and spherical features, the Au surface became superhydrophobic with a CA of 154° and a fluence of 1.2 J/cm<sup>2</sup>. In contrast to the untreated/control surface, all produced surface structures can inhibit *Escherichia coli* adherence. These results demonstrate that fs-LIPSSs have superior antibacterial effectiveness. Table 1 summarizes some compelling findings from recent research that highlight the importance of texture design and LST for surface wettability. Biff et al. [30] explored the wettability characteristics of superelastic NiTi, a key material in biomedical applications, using an fs laser to texture the material surface. The experiments were conducted in ambient air at different laser powers (1 and 13 W) and scanning speeds (2 and 4 m/s). At the lower power level (1 W), micropatterns characterized by ripple-like formations devoid of holes appeared. These ripples were notably smaller than the diameter of the incident laser beam, suggesting a role of factors other than the beam diameter alone. Consequently, the low pulse energy effectively produced a smooth surface. At low energy levels (10 μJ), the laser-patterned surface showed a slightly more regular submicrometer surface morphology than the initial NiTi surface. When the power increased to 13 W (i.e., the pulse energy increased to 170 μJ),

the ripple-like formations were overlapped with a microgroove-like structure. Intensive material ablation promotes the formation of irregular surfaces, indicating that higher power (13 W) generates more visible grooves and removes more of the material than lower power. Consequently, surfaces treated at higher power ( $P = 13$  W) exhibit rougher characteristics than the original surface. Meanwhile, increasing the scanning speed from 2 to 4 m/s decreased the linear energy density  $E$  from 0.5 to 0.25 J/m, thereby reducing the average roughness ( $S_a$ ) values at 1 W. However, this trend was not preserved at a high laser power (13 W) as the  $S_a$  values remained within a similar range, likely because the energy has a threshold. In actuality, increasing the scanning speed from 2 to 4 m/s reduced the  $E$  from 6.5 to 3.25 J/m. By adjusting the laser power and scanning speed, the initial  $S_a$  of 0.41  $\mu\text{m}$  could be reduced to 0.28  $\mu\text{m}$  or increased to 0.62  $\mu\text{m}$ . The CA increased with increasing roughness of the 1 and 13 W samples, indicating a decrease in surface wettability. The CAs of the laser-textured surfaces depended on the irradiation energy; at the lowest energy, the CA was not substantially altered from that of the untreated surface ( $\sim 70^\circ$ ). As the energy increased, the CA rose to  $131^\circ$ , indicating the reduced wettability of the laser-textured surface [30].

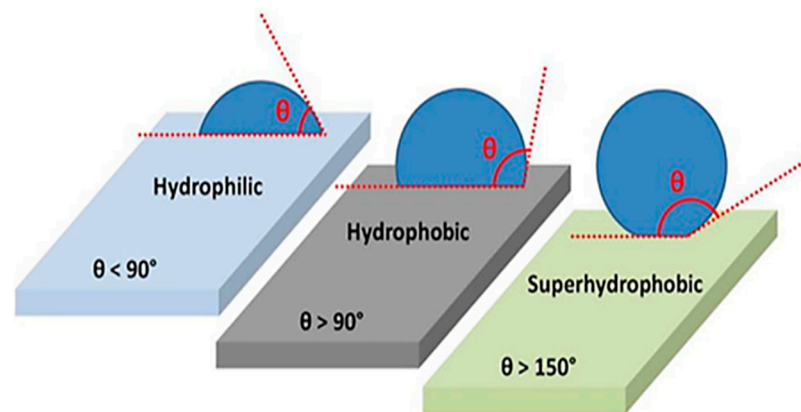


**Figure 4.** A diagram illustrating the contact angles observed on different surfaces [31].

**Table 1.** Overview of the extreme wetting of several materials fabricated through LST.

Material	Laser Fluence ( $\text{J}/\text{cm}^2$ ) or Power	Wavelength (nm)	Repetition (kHz)	Pulse Duration	Contact Angle	Type	Conclusion	Ref
Stainless steel	-	1046	-	9 ns	-	Groove-type	The surface of the microstructure became hydrophobic as the repetition number increased while the frequency was maintained.	[18]
	-	-	-	30 fs	$22.2^\circ$ , $22.8^\circ$ , $23.2^\circ$	Three textures: square, parallel, and perpendicular	Surface hydrophilicity increased. LST demonstrated a clear ability to reduce wear rate and COF.	[19]
	2.04/-	-	5	150 fs	$116.5^\circ$	Nanoperiodic and microperiodic ripples	Materials became hydrophobic as the number of pulses increased.	[23]

Table 1. Cont.

Material	Laser Fluence (J/cm <sup>2</sup> ) or Power	Wavelength (nm)	Repetition (kHz)	Pulse Duration	Contact Angle	Type	Conclusion	Ref
	0.36, 1.14, 2.33/-	-	1000	-	120°	Microgrooves	The surface changed from hydrophilic to hydrophobic and became superhydrophobic when laser processing was performed with the highest repetition rate.	[24]
Titanium surface	-	355	30	20 ns	153.2°	Crosshatch pattern	Wettability could be effectively shifted between superhydrophobicity and superhydrophobicity several times.	[20]
Nickel-based superalloy (C-263)	-	532	-	-	-	Four waviness patterns	A hydrophobic surface was obtained, and the surface roughness of the textured surface increased by 92%.	[21]
Ti-6Al-4V	4.07, 5.09, 6.11, 7.13, 8.14, 9.17/-	-	65	65 ns	-	Micropillars	The most effective topography construction for a superhydrophobic regime was pillar-based with fluences of 5.09 and 6.11 J/cm <sup>2</sup>	[22]
	2.04	-	5	150 fs	116.5°	Nanoperiodic and microperiodic ripples	Materials became hydrophobic as the number of pulses increased	[23]
TiO <sub>2</sub>	-	-	-	-	Low CA of <4°	Microdimples	After laser texturing, all samples displayed superhydrophilic behavior	[25]
steel	0.12, 0.2, 0.5, 1	1030	500, 1000, 2000	340 fs	92° ± 2° to 136° ± 6°; some surfaces presented CAs of >150°	Ripples, grooves, and spikes	A hydrophobic surface was obtained	[26]
CVD diamond material	-	1064	200	100 ns	-	-	The surface roughness values of Sa and Sz increased with the increase in the average laser power and decreased with the increase in laser filling pitch and scanning speed; an exception occurred at a scanning speed of 30 mm/s and filling pitch of 3 mm	[27]

Table 1. Cont.

Material	Laser Fluence (J/cm <sup>2</sup> ) or Power	Wavelength (nm)	Repetition (kHz)	Pulse Duration	Contact Angle	Type	Conclusion	Ref
crystalline InP	125/-	266	0.010	5 ns	-	Ripple	Roughness increased with the increase in laser shots, and the duration of ripple pattern decreased	[28]
gold	0.08–3	800	1	30 fs	10 8°–15 4°	Microstructure/nanostructure	The surface changed from hydrophilic to hydrophobic	[29]
NiT	15	1028	Single pulse: 200 kHz	210 fs–10 ps	131°	Microstructure/nanostructure	The surface changed from hydrophilic to hydrophobic	[30]

## 6. COF and Wear Resistance

Dunn et al. [32] employed a 1064 nm pulsed nanosecond fiber laser to fabricate contacts with texture grade 316 stainless and low-alloy carbon steels. The laser pulse duration and energy were 220 ns and 0.71 mJ, respectively. Short pulse separations combined with single-pass laser texturing of both contacting surfaces readily yielded a high static COF exceeding 1.25, which was 346% higher than the COF of untextured samples obtained at normal pressures of 50 and 100 MPa. The large plastic deformation caused by high normal pressures—which were reached at 100 MPa normal pressure with textures of up to 62.5 m pulse separation—was connected to the high static COF. The high COF observed at low pulse separations is believed to be due to the effective interlocking of two surface textures enabled by the plastic deformation induced by high normal pressure. The number of surface features that could securely interlock decreased with increasing pulse separation, resulting in an untextured surface with a reduced COF. Lu et al. [33] investigated the effect of LST on the COF and wear resistance of chromium alloys. Different patterns were created, such as microdimples, microgrooves, and microgrids. An Nd–YAG laser with a 100 kHz frequency, 600 ps pulse duration, 1064 nm wavelength, and 15.6 W maximum power was employed to create textures on the sample surfaces. The following conclusion was reached: under dry conditions, the wear rates of the samples with microdimples, microgrooves, and microgrids were approximately 18%, 37%, and 57% lower than those of the untextured sample, respectively. All laser-textured surfaces had a lower COF than the untextured surfaces. The COF of the laser-textured surfaces initially decreased and then increased with decreasing texture density. Reduced COF can increase wear resistance. Using a unidirectional pin-on-disk tribometer, Segu and Hwang [34] examined the effects of multishaped LST using circles and ellipses, circles and triangles, and circles and squares. The pulsed Q switch Nd:YAG laser used for the surface texturing of steel had the following specifications: 200 ns pulse duration, 1 mJ pulse energy, 15 kHz PRR, and 24 W power. This study demonstrated that under dry and lubricated conditions, the COF of the multishaped textured surface was less extreme and more stable than that of the received sample surface. The COFs of all surfaces decreased with increasing sliding speed. Wear debris was visible at the interface of untextured surfaces and was trapped by dimples on textured surfaces. Shi et al. [35] investigated the macroscale tribological performance of graphene on textured M2 steel surfaces. The LST approach was employed to create microgrooves on M2 steel surfaces with various area ratios. A thin layer of graphene flakes was then applied using a graphene-containing ethanol solution on the textured surfaces. Subsequently, the surface was prepared with parallel microgrooves using an Nd:YAG laser device with a maximum laser power of 350 W and wavelength of 1064 nm. Three samples, each with a different groove period corresponding to a different groove area ratio (groove area/total area ratio), of the textured substrates were generated. The findings of the above work demonstrated that the wear resistance of the textured samples was effectively improved by graphene

lubrication with suitable groove area ratios (35% and 56%) relative to that of bare M2 steel. This improvement was due to the creation of a protective carbon layer and the effective entrapment of wear debris. Graphene, especially at a groove area of 35%, was sufficient to reduce friction and provide the necessary support for high-contact stress, thereby improving friction behavior. The sample with a 35% groove area can sustain 870 sliding cycles at a low COF (0.22), whereas the bare M2 steel surface can only sustain 80 sliding cycles. Furthermore, an 80% reduction in the wear rate considerably enhanced the wear resistance. Arenas et al. [36] studied the tribological behavior and performance of the Ti-6Al-4V alloy. LST was used to create cross-groove patterns on the alloy, and graphene or MoS<sub>2</sub> was subsequently applied. A pulsed Nd:YVO<sub>4</sub> laser with a wavelength of 1064 nm and pulse duration of 10 ps was used for texturing. The sample was textured using energy pulses of 8 J repeated at a 10 kHz rate. The surface was scanned at 1.2 mm/s. Crossing these grooves produced shapes resembling rhombuses. Crossing angles of 60° or 45° were produced to obtain rhombus patterns. The textured surface area had densities of 18%, 40%, and 64% for both crossing angles. The textured and nontextured surfaces exhibited the same poor tribological performance in the absence of lubrication, with a very high COF of approximately 0.6. However, the COF of the textured surfaces coated with graphene or MoS<sub>2</sub> decreased to approximately 0.2. Li et al. [37] reported the use of LS to enhance the antifriction properties of 304 stainless steel. The sample was fabricated using a nanosecond fiber laser with a continuously adjustable repetition frequency of 30–60 kHz, maximum average power of 20 W, pulse length of 200 ns, and wavelength of 1064 nm. The antifriction characteristics of the 304 stainless steel surface can be enhanced by adjusting the morphology of the texture by laser parameter optimization. By changing the textural morphology of the 304 stainless steel surfaces, enhancing the laser parameters can enhance antifriction effectiveness. The experimental findings showed that decelerating scanning, reducing repetition frequency, and decreasing laser-beam line spacing while maintaining the appropriate lattice spacing resulted in a gradual increase in texture depth and enhancement in debris collection, leading to a low COF because the texture trapped impurities, such as abrasive dust. This effect thus reduced the surface roughness of the substrate material while decreasing abrasive wear on the surface. The laser parameters affected the structure size and shape. Consequently, a surface made of stainless steel with strong antifriction features was produced when the laser power was set to 0.3 W, the repetition frequency was set to 50 kHz, the scanning speed was set to 80 mm/s, the laser-beam line spacing was set to 1 m, the lattice spacing was set to 200 μm, and the number of processing times was two. The three types of wear—abrasive, fatigue, and adhesive—simultaneously occurred in the absence of LST. Fatigue wear was primarily visible on rough surfaces. The designed texture effectively collected the wear debris generated during wear, thereby reducing the occurrence of adhesive and abrasive wear. This effect enhanced the material's ability to reduce friction on its surface. Mishra et al. [38] investigated the friction and wear behaviors of a WC/Co laser-textured surface by performing an open tribology test. Tests were conducted on laser-textured WC/Co surfaces to evaluate the tribological performances of hard coatings deposited through physical vapor deposition. Nanosecond solid-state Nd:YAG was used to apply microhole textures to the surfaces of the WC/Co pins. Furthermore, AlCrN and AlTiN monolayers were applied to the laser-textured pins. The sample was then subjected to loading, speed, and sliding time tests using an open-pin tribotester. The first set of requirements was a moderate sliding time, high speed, and low load of 30 s, 100 m/min, and 500 N, respectively. The second set of requirements was a heavy load, low speed, and short sliding duration of 1000 N, 40 m/min, and 10 s, respectively. Results revealed that the continual development of the transfer layers produced severe adhesion over simple uncoated pins for low load. The COF of the textured coated surfaces was reduced under extreme tribological conditions of low and high loads. AlCrN-textured coated surfaces exhibited a maximum reduction of 27% under high-load conditions. In terms of the wear mechanism, unstable growth of transfer layers and transverse cracks occurred on untextured surfaces but were absent on coated or uncoated textured surfaces. In addition, the textured coated surfaces did not experience

severe adhesion or frequently developed ridges on their surfaces. Table 2 summarizes some compelling findings from recent research that highlight the importance of texture design and LST for COF.

**Table 2.** Overview of the coefficients of friction and wear resistance of several materials produced through LST.

Material	Laser Fluence (J/cm <sup>2</sup> ) or Power	Wavelength (nm)	Pulse Duration	COF	Type	Conclusion	Ref
316 stainless steel	167/-	1064	220 ns	1.25	-	A very high static COF of >1.25 was obtained.	[32]
Chromium alloys	-/15.6 W	-	600 ps	Lower COF than the as-received surfaces	-	Under dry conditions, the wear rate and COF of the textured samples and were lower than those of the sample received.	[33]
Steel	-/24 W	1064	200 ns	Less extreme and more stable than the unpatterned surface	Circle and ellipse, circle and triangle, and circle and square	The multishaped pattern surface performed better than the unpatterned surface in terms of stability and COF under dry and lubricated conditions.	[34]
M2 steel surfaces	-/350 W	1064	-	Low COF of approximately 0.22	Parallel microgrooves	With a percentage of 35% groove areas, there was enough graphene to minimize friction, and an 80% reduction in the wear rate considerably enhanced the wear resistance.	[35]
Ti-6Al-4V	-	1064	-	Low COF of approximately 0.2	Cross-groove patterns	The COF dropped to approximately 0.2 for patterned surfaces coated with graphene or MoS <sub>2</sub> .	[36]
304 stainless steel	-/20 W	1064	200 ns	Low COF	-	A low COF was obtained.	[37]
WC/Co	-	-	-	COF decreased	Microholes	COF decreased for coated patterned surfaces under high and low load conditions.	[38]

Texturing is a commonly used procedure that alters the surface properties by adjusting the surface texture and roughness. Laser beams generate tiny patterns on surfaces through precise ablation and the removal of surface layers. Based on the sizes of the generated features, texturing is categorized into microsurface and nanosurface texturing. Microsurface texturing produces micron-scale surface features such as asperities, patterns, and dimples, aiming to enhance properties such as wettability, optical characteristics, antimicrobial resistance, wear resistance, low-friction capability, and corrosion resistance in harsh environments. With similar goals, nanosurface texturing produces nanosized structures that improve the antireflective transparency and hence the optical properties of surfaces. These texturing techniques are applied in various industries and devices such as magnetic

storage drives, metallic and dielectric films, nanomaterial processing, engine components, hydraulic equipment, thrust bearings, and seals [39].

Laser texturing with ultrashort laser pulses, typically in the fs range, is a standout method for surface modification. The underlying theory states that ultrashort-pulsed laser radiation induces two-photon absorption on the surface. The consequent photon-to-electron energy transfer causes high-temperature electronic vibrations that transfer energy to the surrounding electrons and lattice, elevating the overall surface temperature. When the damage threshold energy is reached, the lattice of the surface material begins to fracture, releasing high-energy atoms and electrons that rapidly disperse. Consequently, a plasma in the irradiated zone can form through direct material vaporization or bubble formation. The shock waves resulting from bubble expansion induce structural transformations on the surface. Increasing the laser power or energy increases the size and pressure of the bubbles, consequently expanding the depth and width of shock-induced ruptures and enlarging the surface pores [30,40,41].

Laser texturing depends on many parameters, including the characteristics of the power source, the substrate material properties, the laser focusing parameters, pulse duration, spot diameter, scanning rate, repetition rate, and pulse length. By manipulating these parameters, researchers have created various surface patterns such as grooves, dimples, and intricate designs that enhance the surface roughness and wettability of materials. Various types of grooves, such as grid, circular, and asterisk configurations, have enhanced the properties related to friction and wear resistance [40].

#### *6.1. Effects of Laser Parameters on Surface Roughness and Wettability*

Wettability is governed by both chemical composition and surface morphology and largely depends on the surface microstructure, which can be manipulated by changing the LST parameters [42,43]. The laser fluence, pitch or overlap, and surface patterns directly impact the wettability of a surface [44–47]. Specifically, increasing the laser fluence increases the amount of molten material removed, creating deep valleys and pronounced ridges that increase the surface roughness. Adjusting the scanning speed or distance also enhances the surface roughness, as it increases the overlap and hence the proximity of holes. Moreover, reducing the pulse repetition frequency can augment the pulse energy, thereby intensifying the melt jet. The laser parameters and surface roughness largely influence the wettability outcomes [42]. Sierra, Gemini, and Jalil have shown that at high laser fluences, superhydrophobic surfaces develop on various materials. Laser power intensity is an especially critical parameter of LST as it primarily dictates the resulting surface texture. In both ablation- and interference-based LSTs, the laser power intensity directly affects the amount of laser energy delivered, determining the dimensions and shape of texture features and the extent of the HAZ [40]. Higher laser intensities are reported to increase the depth and diameter of texture features and accentuate the surface roughening effects, thereby impacting the friction behavior. The laser power intensity of ablation-based LST shapes the geometry (depth and size) of the texture features [40]. Chen et al. and Biff et al. [30] demonstrated that besides increasing the surface roughness, a high laser power converts hydrophilic Ni-based superalloy (C-263) and NiTi surfaces to hydrophobic surfaces. The laser scanning speed, which defines the scanning rate of the laser beam over the substrate, influences both the heat input and cooling rate of the processed material. Slower scanning speeds facilitate deeper penetration and enlarge the HAZ. Conversely, faster scanning speeds enable deeper penetration while minimizing the size of the HAZ [39]. Prakash et al. [21] and Chen et al. [27] demonstrated that increasing the scanning speed effectively reduces the surface roughness. LST processes can modify the geometry of surface features with multiple pulses. The size, depth, and shape of surface features also critically depend on the number of pulses. Specifically, increasing the pulse number affects the depth, height, inner diameter, and outer diameter of craters formed via laser ablation. As the number of pulses increases, the crater height rises while the inner diameter decreases [40]. Bizi-Bardoki et al. [23] and Kumar and Soni [28] reported that

increasing the pulse number heightens the surface roughness and induces a transition from hydrophilic to hydrophobic surface properties.

6.2. Effects of Laser Parameters on Surface COF and Wear Resistance

The laser parameters affect not only the density and shape of surface textures but also the friction and wear characteristics of surfaces. Textured surfaces usually exhibit lower COFs than untextured surfaces because wear debris becomes trapped in the texture features and diminishes the friction [40]. Ahmed et al. [19] and Lu et al. [33] similarly reported lower COFs and higher wear resistance on various textured surfaces than on their untextured counterparts. The pulse separation additionally affects the COFs of material surfaces. Dunn et al. [32] examined the impact of pulse separation on the surface COFs. They attributed the heightened COFs observed at lower pulse separations to effective interlocking between the surface textures, facilitated by plastic deformation under sufficiently high normal pressures. Increasing the pulse separation decreased the number of surface features that could securely interlock. The resulting surface resembled that of an untextured surface with a lower COF. Sliding speed is another influencer of surface friction. Segu and Hwang [34] found that the COFs of all surfaces in their study decreased with increasing sliding speed. Notably, they observed that wear debris at the interfaces of untextured surfaces was effectively trapped in dimples on the textured surfaces.

Figure 5 illustrates some laser parameters that affect surface wettability and roughness. Figures 6 and 7 illustrate some of the laser parameters that affect the COF of the surface and the effect of laser texturing shape on the COF, wear rate, and surface roughness.

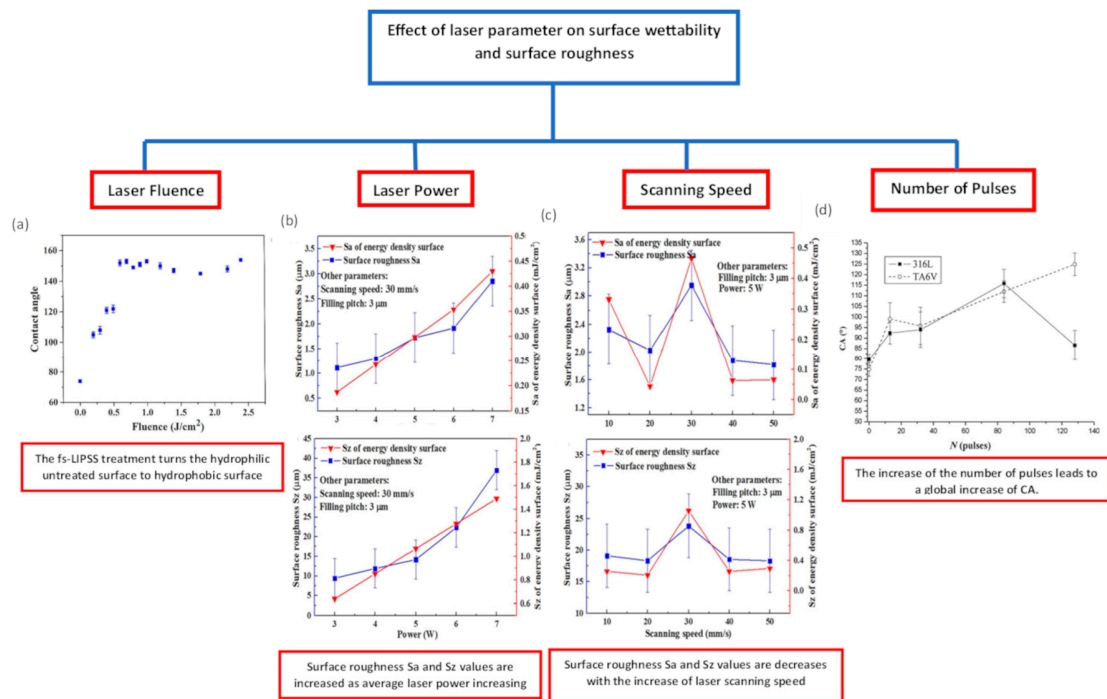


**Figure 5.** Some laser parameters that affect wettability and surface roughness after surface texturing. (a) CA measurements as a function of laser fluence [29]. (b) Surface roughness Sa and Sz values as a function of average laser power [27]. (c) Surface roughness Sa and Sz values as functions of scanning speed [27]. (d) Water CAs of Ti-6Al-V and AISI 316L stainless steel surfaces as functions of the number of pulses [23].

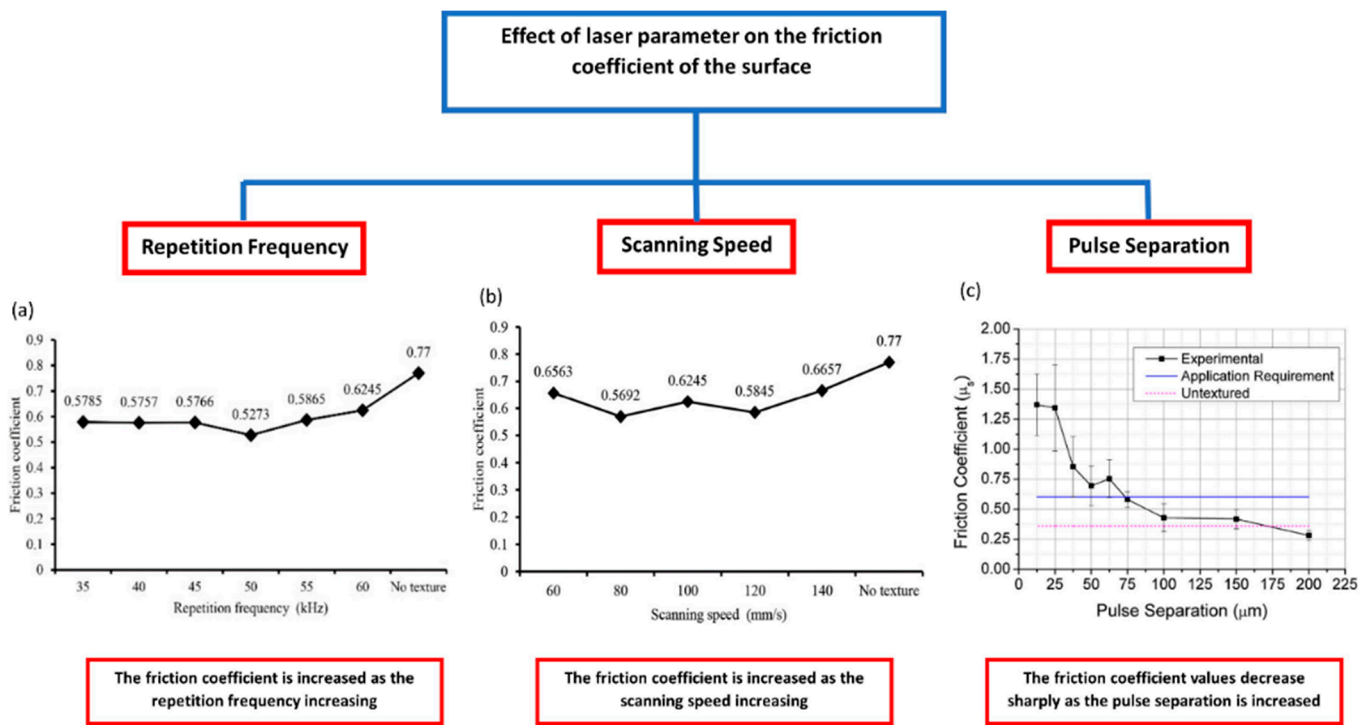


Figure 6. Relation between the coefficient of friction and (a) repetition frequency [37], (b) scanning speed [37], and (c) pulse separation [32].

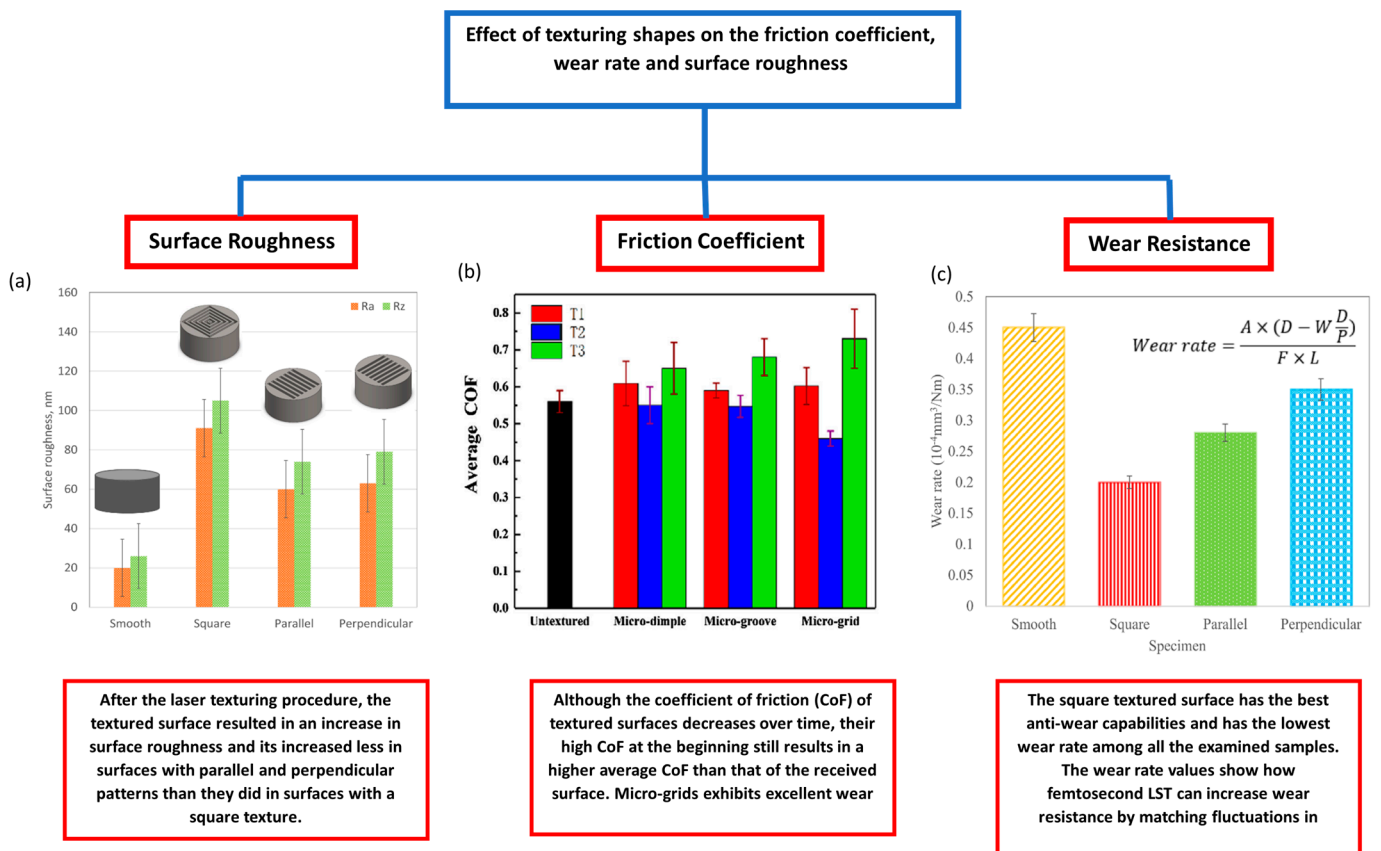


Figure 7. (a) Surface roughness of several laser-textured designs [19]. (b) Coefficients of friction of several laser-textured designs [33]. (c) Wear rates of several laser-textured designs [19].

## 7. Summary and Outlook

Surface texturing is a commonly used technique for enhancing the surface quality of materials. LST is the most well-known technique in this regard. Among surface texturing techniques, LST is a superior technology for application in the aerospace, automotive, biomedical, and semiconductor device production industries because it can be used to manufacture microsurface or nanosurface textures for various substrate materials. Different surface modification parameters provide substrates with various properties. Consequently, the parameters used during modification must be slightly modified to meet the requirements of substrate applications.

**Funding:** This research received no external funding.

**Data Availability Statement:** All data generated or analyzed during this study are included in this article.

**Conflicts of Interest:** The author declare no conflicts of interest.

## References

- Guo, B.; Sun, J.; Hua, Y.; Zhan, N.; Jia, J.; Chu, K. Femtosecond laser micro/nano-manufacturing: Theories, measurements, methods, and applications. *Nanomanuf. Metrol.* **2020**, *3*, 26–67. [\[CrossRef\]](#)
- Tan, D.; Sharafudeen, K.N.; Yue, Y.; Qiu, J. Femtosecond laser induced phenomena in transparent solid materials: Fundamentals and applications. *Prog. Mater. Sci.* **2016**, *76*, 154–228. [\[CrossRef\]](#)
- Bharatish, A.; Soundarapandian, S. Influence of femtosecond laser parameters and environment on surface texture characteristics of metals and nonmetals—State of the art. *Lasers Manuf. Mater. Process.* **2018**, *5*, 143–167. [\[CrossRef\]](#)
- Shugaev, M.V.; Wu, C.; Armbruster, O.; Naghilou, A.; Brouwer, N.; Ivanov, D.S.; Derrien, T.J.-Y.; Bulgakova, N.M.; Kautek, W.; Rethfeld, B.; et al. Fundamentals of ultrafast laser–material interaction. *MRS Bull.* **2016**, *41*, 960–968. [\[CrossRef\]](#)
- Lin, Z.; Hong, M. Femtosecond Laser Precision Engineering: From Micron, Submicron, to Nanoscale. *Ultrafast Sci.* **2021**, *2021*. [\[CrossRef\]](#)
- Sundaram, S.K.; Mazur, E. Inducing and probing non-thermal transitions in semiconductors using femtosecond laser pulses. *Nat. Mater.* **2002**, *1*, 217–224. [\[CrossRef\]](#) [\[PubMed\]](#)
- Balling, P.; Schou, J. Femtosecond-laser ablation dynamics of dielectrics: Basics and applications for thin films. *Rep. Prog. Phys. Phys. Soc.* **2013**, *76*, 036502. [\[CrossRef\]](#) [\[PubMed\]](#)
- Stuart, B.C.; Feit, M.D.; Herman, S.; Rubenchik, A.M.; Shore, B.W.; Perry, M.D. Nanosecond-to-femtosecond laser-induced breakdown in dielectrics. *Phys. Rev. B Condens. Matter* **1996**, *53*, 1749–1761. [\[CrossRef\]](#) [\[PubMed\]](#)
- Rousse, A.; Rischel, C.; Fourmaux, S.; Uschmann, I.; Sebban, S.; Grillon, G.; Balcou, P.; Forster, E.; Geindre, J.; Audebert, P.; et al. Non-thermal melting in semiconductors measured at femtosecond resolution. *Nature* **2001**, *410*, 65–68. [\[CrossRef\]](#)
- Hase, M.; Fons, P.; Mitrofanov, K.; Kolobov, A.V.; Tominaga, J. Femtosecond structural transformation of phase-change materials far from equilibrium monitored by coherent phonons. *Nat. Commun.* **2015**, *6*, 8367. [\[CrossRef\]](#)
- Brown, M.S.; Arnold, C.B. Fundamentals laser-material interaction and application to multiscale surface modification. In *Laser Precision Microfabrication*; Springer: Berlin/Heidelberg, Germany, 2010; pp. 91–120.
- Moskal, D.; Martan, J.; Honner, M. Scanning strategies in laser surface texturing: A review. *Micromachines* **2023**, *14*, 1241. [\[CrossRef\]](#) [\[PubMed\]](#)
- Zhang, L.; Lin, N.; Zou, J.; Lin, X.; Liu, Z.; Yuan, S.; Yu, Y.; Wang, Z.; Zeng, Q.; Chen, W.; et al. Super-hydrophobicity and corrosion resistance of laser surface textured AISI 304 stainless steel decorated with hexadecyltrimethoxysilane (HDTMS). *Opt. Laser Technol.* **2020**, *127*, 106146. [\[CrossRef\]](#)
- Luo, X.; Tian, Z.; Chen, C.; Jiang, G.; Hu, X.; Wang, L.; Peng, R.; Zhang, H.; Zhong, M. Laser-textured high-throughput hydrophobic/superhydrophobic SERS platform for fish drugs residue detection. *Opt. Laser Technol.* **2022**, *152*, 108075. [\[CrossRef\]](#)
- He, C.; Yang, S.; Zheng, M. Analysis of synergistic friction reduction effect on micro-textured cemented carbide surface by laser processing. *Opt. Laser Technol.* **2022**, *155*, 108343. [\[CrossRef\]](#)
- Chen, X.; Lei, Z.; Chen, Y.; Jiang, M.; Jiang, N.; Bi, J.; Lin, S. Enhanced wetting behavior using femtosecond laser-textured surface in laser welding-brazing of Ti/Al butt joint. *Opt. Laser Technol.* **2021**, *142*, 107212. [\[CrossRef\]](#)
- Mahayuddin, N.; Wahab, J.A.; Salleh, M.; Roduan, S.F.; Chen, H.K. Surface texturing method and roughness effect on the substrate performance: A short review. *J. Tribol.* **2020**, *27*, 8–18.
- Moldovan, E.R.; Doria, C.C.C.; Ocaña, J.L.; Baltés, L.S.; Stanciu, E.M.; Croitoru, C.; Pascu, A.; Roata, I.C.; Tiorean, M.H. Wettability and surface roughness analysis of laser surface texturing of AISI 430 stainless steel. *Materials* **2022**, *15*, 2955. [\[CrossRef\]](#) [\[PubMed\]](#)
- Ahmed, Y.S.S.; DePaiva, J.M.; Amorim, F.L.; Torres, R.D.; de Rossi, W.; Veldhuis, S.C. Laser surface texturing and characterization of austenitic stainless steel for the improvement of its surface properties. *Int. J. Adv. Manuf. Technol.* **2021**, *115*, 1795–1808. [\[CrossRef\]](#)
- Wang, Q.; Wang, H.; Zhu, Z.; Xiang, N.; Wang, Z.; Sun, G. Switchable wettability control of titanium via facile nanosecond laser-based surface texturing. *Surf. Interfaces* **2021**, *24*, 101122. [\[CrossRef\]](#)
- Prakash, F.P.; Jeyaprakash, N.; Duraiselvam, M.; Prabu, G.; Yang, C.-H. Droplet spreading and wettability of laser textured c-263 based nickel superalloy. *Surf. Coat. Technol.* **2020**, *397*, 126055. [\[CrossRef\]](#)

22. Sierra, D.R.; Edwardson, S.; Dearden, G. Laser surface texturing of titanium with thermal post-processing for improved wettability properties. *Procedia CIRP* **2018**, *74*, 362–366. [[CrossRef](#)]
23. Bizi-Bandoki, P.; Benayoun, S.; Valette, S.; Beaugiraud, B.; Audouard, E. Modifications of roughness and wettability properties of metals induced by femtosecond laser treatment. *Appl. Surf. Sci.* **2011**, *257*, 5213–5218. [[CrossRef](#)]
24. Gemini, L.; Faucon, M.; Romoli, L.; Kling, R. High throughput laser texturing of super-hydrophobic surfaces on steel. In Proceedings of the Laser-Based Micro-and Nanoprocessing XI, San Francisco, CA, USA, 31 January–2 February 2017.
25. Yusuf, Y.; Ghazali, M.J.; Abdollah, M.F.B.; Otsuka, Y.; Nakamura, S.; Pembuatan, F.T.K.M.d. Superhydrophilicity of laser surface textured TiO<sub>2</sub> coating for self-cleaning surfaces. In *Proceedings of Mechanical Engineering Research Day 2019*; Centre for Advanced Research on Energy: Melaka, Malaysia, 2019; pp. 342–343.
26. Baron, C.F.; Mimidis, A.; Puerto, D.; Skoulas, E.; Stratakis, E.; Solis, J.; Siegel, J. Biomimetic surface structures in steel fabricated with femtosecond laser pulses: Influence of laser rescanning on morphology and wettability. *Beilstein J. Nanotechnol.* **2018**, *9*, 2802–2812. [[CrossRef](#)] [[PubMed](#)]
27. Chen, N.; Li, Z.; Wu, Y.; Zhao, G.; Li, L.; He, N. Investigating the ablation depth and surface roughness of laser-induced nano-ablation of CVD diamond material. *Precis. Eng.* **2019**, *57*, 220–228. [[CrossRef](#)]
28. Kumar, B.; Soni, R.K. Submicrometre periodic surface structures in InP induced by nanosecond UV laser pulses. *J. Phys. D* **2008**, *41*, 155303. [[CrossRef](#)]
29. Jalil, S.A.; Akram, M.; Bhat, J.A.; Hayes, J.J.; Singh, S.C.; ElKabbash, M.; Guo, C. Creating superhydrophobic and antibacterial surfaces on gold by femtosecond laser pulses. *Appl. Surf. Sci.* **2020**, *506*, 144952. [[CrossRef](#)]
30. Biffi, C.A.; Fiocchi, J.; Rancan, M.; Gambaro, S.; Cirisano, F.; Armelao, L.; Tuissi, A. Ultrashort laser texturing of superelastic NiTi: Effect of laser power and scanning speed on surface morphology, composition and wettability. *Metals* **2023**, *13*, 381. [[CrossRef](#)]
31. Oberli, L.; Caruso, D.; Hall, C.; Fabretto, M.; Murphy, P.J.; Evans, D. Condensation and freezing of droplets on superhydrophobic surfaces. *Adv. Colloid Interface Sci.* **2014**, *210*, 47–57. [[CrossRef](#)] [[PubMed](#)]
32. Dunn, A.; Wlodarczyk, K.L.; Carstensen, J.V.; Hansen, E.B.; Gabzdyl, J.; Harrison, P.M.; Shephard, J.D.; Hand, D.P. Laser surface texturing for high friction contacts. *Appl. Surf. Sci.* **2015**, *357*, 2313–2319. [[CrossRef](#)]
33. Lu, L.; Zhang, Z.; Guan, Y.; Zheng, H. Comparison of the effect of typical patterns on friction and wear properties of chromium alloy prepared by laser surface texturing. *Opt. Laser Technol.* **2018**, *106*, 272–279. [[CrossRef](#)]
34. Segu, D.Z.; Hwang, P. Effectiveness of multi-shape laser surface texturing in the reduction of friction under lubrication regime. *Ind. Lubr. Tribol.* **2016**, *68*, 116–124. [[CrossRef](#)]
35. Shi, Z.; Shum, P.; Wasy, A.; Zhou, Z.; Li, L.K.-Y. Tribological performance of few layers graphene on textured m2 steel surfaces. *Surf. Coat. Technol.* **2016**, *296*, 164–170. [[CrossRef](#)]
36. Arenas, M.A.; Ahuir-Torres, J.I.; García, I.; Carvajal, H.; de Damborenea, J. Tribological behaviour of laser textured Ti–6Al–4V alloy coated with MoS<sub>2</sub> and graphene. *Tribol. Int.* **2018**, *128*, 240–247. [[CrossRef](#)]
37. Li, X.; Li, G.; Lei, Y.; Gao, L.; Zhang, L.; Yang, K. Influence of laser surface texture on the anti-friction properties of 304 stainless steel. *Machines* **2023**, *11*, 473. [[CrossRef](#)]
38. Mishra, S.K.; Ghosh, S.; Aravindan, S. Investigations into friction and wear behavior of AlTiN and AlCrN coatings deposited on laser textured WC/co using novel open tribometer tests. *Surf. Coat. Technol.* **2020**, *387*, 125513. [[CrossRef](#)]
39. Rufuss, S.A.D.D.W.; Jain, A.; Kandasamy, J.; Singhal, M. Laser processing techniques for surface property enhancement: Focus on material advancement. *Surf. Interfaces* **2023**, *42*, 103293.
40. Mao, B.; Siddaiah, A.; Liao, Y.; Menezes, P.L. Laser surface texturing and related techniques for enhancing tribological performance of engineering materials: A review. *J. Manuf. Process.* **2020**, *53*, 153–173. [[CrossRef](#)]
41. Liang, C.; Wang, H.; Yang, J.; Li, B.; Yang, Y.; Li, H. Biocompatibility of the micro-patterned NiTi surface produced by femtosecond laser. *Appl. Surf. Sci.* **2012**, *261*, 337–342. [[CrossRef](#)]
42. Liu, Z.; Niu, T.; Lei, Y.; Luo, Y. Metal surface wettability modification by nanosecond laser surface texturing: A review. *Biosurf. Biotribol.* **2022**, *8*, 95–120. [[CrossRef](#)]
43. MacGregor-Ramiassa, M.N.; Vasilev, K. Questions and answers on the wettability of nano-engineered surfaces. *Adv. Mater. Interfaces* **2017**, *4*, 1700381. [[CrossRef](#)]
44. Sarbada, S.; Shin, Y.C. Superhydrophobic contoured surfaces created on metal and polymer using a femtosecond laser. *Appl. Surf. Sci.* **2017**, *405*, 465–475. [[CrossRef](#)]
45. Yang, C.j.; Mei, X.s.; Tian, Y.l.; Zhang, D.w.; Li, Y.; Liu, X.p. Modification of wettability property of titanium by laser texturing. *Int. J. Adv. Manuf. Technol.* **2016**, *87*, 1663–1670. [[CrossRef](#)]
46. Cunha, A.; Serro, A.P.; Oliveira, V.; Almeida, A.; Vilar, R.; Durrieu, M.-C. Wetting behaviour of femtosecond laser textured ti–6al–4v surfaces. *Appl. Surf. Sci.* **2013**, *265*, 688–696. [[CrossRef](#)]
47. Li, B.; Li, H.; Huang, L.j.; Ren, N.f.; Kong, X. Femtosecond pulsed laser textured titanium surfaces with stable superhydrophilicity and superhydrophobicity. *Appl. Surf. Sci.* **2016**, *389*, 585–593. [[CrossRef](#)]

**Disclaimer/Publisher’s Note:** The statements, opinions and data contained in all publications are solely those of the individual author(s) and contributor(s) and not of MDPI and/or the editor(s). MDPI and/or the editor(s) disclaim responsibility for any injury to people or property resulting from any ideas, methods, instructions or products referred to in the content.